IEEE Access
Multidisciplinary | Rapid Review | Open Access Journal

Received October 22, 2019, accepted November 7, 2019, date of publication November 20, 2019,
date of current version December 16, 2019.

Digital Object Identifier 10.1109/ACCESS.2019.2954708

Analysis of Varicose Veins of Lower Extremities Based on Vascular Endothelial Cell Inflammation Images and Multi-Scale Deep Learning

RUIZONG ZHU[1], HUIPING NIU[2], NINGNING YIN[3], TIANJIAO WU[3], AND YAPEI ZHAO[3]
[1]Department of Clinical Laboratory, Dingzhou People's Hospital, Dingzhou 073000, China
[2]Endoscopy Center, The Second Hospital of Hebei Medical University, Shijiazhuang 050000, China
[3]Department of Ultrasound, The Second Hospital of Hebei Medical University, Shijiazhuang 050000, China

Corresponding author: Yapei Zhao (zhaoyapei1@163.com)

ABSTRACT The doctor determines whether there are lesions in the human body through the diagnosis of medical images, and classifies and identifies the lesions. Therefore, the automatic classification and recognition of medical images has received extensive attention. Since the inflammatory phenomenon of vascular endothelial cells is closely related to the varicose veins of the lower extremities, in order to realize the automatic classification and recognition of varicose veins of the lower extremities, this paper proposes a varicose vein recognition algorithm based on vascular endothelial cell inflammation images and multi-scale deep learning, called MSDCNN. First, we obtained images of vascular endothelial cells in patients with varicose veins of the lower extremities and normal subjects. Second, multiple convolutional layers extract multi-scale features of vascular endothelial cell images. Then, the MFM activation function is used instead of the ReLU activation function to introduce a competitive mechanism that extracts more features that are compact and reduces network layer parameters. Finally, the network uses a 3×3 convolution kernel to improve the network feature extraction capability and use the 1×1 convolution kernel for dimensionality reduction to further streamline network parameters. The experimental results tell us that the network has the advantages of high recognition accuracy, fast running speed, few network parameters, and is suitable for small-embedded devices.

INDEX TERMS Vascular endothelial cells, inflammation, multi-scale deep learning, varicose veins of the lower extremities.

I. INTRODUCTION

With the continuous development of science and technology, digital medicine and digital images are increasingly developing into society. The technologies developed in recent years, such as image processing and virtual reality technology, are slowly being applied in the medical field. Digital medicine as a medicine interdisciplinary research combined with digital art has also achieved rapid development in recent years. The network algorithm designed by Lau *et al.* [1] can achieve a good recognition effect in 1000 images of skin damage. Alzheimer [2] used 3D convolution in order to classify the patients of Alzheimer's disease. Kawahara *et al.* [3] applied a CNN structure to the brain connectivity map obtained from MRI diffusion tensor imaging DTI. Shen *et al.* [4] used three CNNs, each of which used a module patch as input at different scales, and then connected the resulting characteristics of the three CNNs to form the final feature vector. Yuan *et al.* [5] used a multi-stream CNN to classify skin lesions, each working at a different resolution of the image. Al-Antari *et al.* [6] used a structured support vector machine combined with deep learning to segment breast lumps, indicating that the model improves the accuracy and effectiveness of breast image segmentation. Xu *et al.* [7] proposed stacked sparse auto-encoder for automated nuclear detection of breast cancer histopathology, and found that the model is superior to baseline method. Shi *et al.* [8] used a classification framework based on deep polynomial network and

The associate editor coordinating the review of this manuscript and approving it for publication was Yongtao Hao.

multiple kernel learning (MKL) to detect and diagnose ultrasound images of breast, and found that DPN-MKL algorithm is based on small images and ultrasound images. It is superior to commonly used deep learning algorithms in terms of tumor classification.

The varicose veins of the lower extremities are the most common peripheral vascular disease. About 23% of adults suffer from varicose veins of the lower extremities, and the current number has exceeded 25 million [9], [10]. In China, the prevalence of varicose veins has exceeded 8% [11]. In addition to affecting aesthetics, varicose veins can also cause complications, for example, venous edema, skin ulcers and thrombophlebitis, and increase the risk of deep vein thrombosis [12], which can cause disability and the lower labor force. The annual direct cost of treating chronic venous diseases (CVD) in the United States is estimated at $1.5 million to $1 billion [13]–[15]. In the UK, the cost of treating varicose veins has accounted for 2% of total national health expenditure [16]. Traditional treatments for the varicose veins of the lower extremities include conservative and surgical treatment, but the recurrence rate is about 1/3 within 10 years after surgery [17], while minimally invasive treatments such as intravascular laser, radiofrequency ablation, and foam have been developed in recent years [18]–[20]. Therefore, from a long-term perspective, studying the molecular and cellular mechanisms of varietal pathogenesis is of great significance for finding new therapeutic targets and developing new therapeutic strategies.

Vascular endothelial cells (VECs) are a layer of intact monolayers on the inner surface of blood vessels, between the bloodstream and the walls of blood vessels, directly sensing hemodynamic changes. It is a mechanical barrier with many functions such as material transport, autocrine, and paracrine, and it is very relevant to many physiological and pathological processes of the human body. Its structure and function are abnormal in many diseases, especially in the lower limbs. It plays an important role in the occurrence and development of varicose veins. Depopas and Brown [21] introduced the concept of rough set and improved the diagnostic accuracy of the disease through basic information processing of patients with varicose veins of the lower extremities. Chen *et al.* [22] used artificial neural network to generate image classifier, and then carried out automatic analysis of vascular endothelial cell images. This method can classify the images of vascular endothelial cells according to the condition of the disease. James and Allen [23] applied artificial neural network to lower limb vein images by classifying several features of interest by using different pattern classifiers. In order to improve the early diagnosis of the disease, Sorelli *et al.* [24] used a support vector machine to classify the images of vascular endothelial cells effectively. Fu *et al.* [25] proposed to analyze varicose veins in lower extremities by using responsive and prospective neural control mechanisms through grip force sensation. Veinidis *et al.* [26] proposed an unsupervised human motion retrieval algorithm based on three-dimensional grid sequence to determine whether there is a varicose vein in the lower extremity.

However, there are some problems in the above algorithms, such as the small amount of data of vascular endothelial cells, the difficulty of network training, and the poor fitting effect. Deep learning adopts hierarchical feature extraction structure, and extracts more in-depth and abstract features by layer by layer abstraction of input images from low level to high level, as well as sequential iteration in the training process, so as to discover the most essential attributes of data. Therefore, this paper adopts the deep learning method to extract and classify features. This paper uses the multi-scale deep learning algorithm to extract the characteristics of vascular endothelial cell inflammation images, and then classifies and recognizes varicose veins of lower extremities. Multiple convolutional layers extracted multi-scale features of vascular endothelial cell images. At the same time, the MFM activation function is used instead of the ReLU activation function to introduce a competitive mechanism that can extract more features that are compact and reduce network layer parameters. The network adopts a 3×3 convolution kernel and uses a 1×1 convolution kernel for dimensionality reduction, which can be used to improve network feature extraction capability and further streamline network parameters.

Specifically, the technical contributions of our paper can be concluded as follows:

In this paper, vascular endothelial cells were used as research objects to classify and identify varicose veins of lower extremities by extracting the inflammatory features of endothelial cells. The experimental results show that the network has the advantages of high recognition accuracy, fast running speed, few network parameters, and is suitable for small-embedded devices.

The rest of our paper was organized as follows. Related work was introduced in Section II. Section III described the multi-scale deep convolutional network algorithm proposed in this paper. In section IV, we designed experimental results, and analysis for experimental results was discussed in detail. Finally, Section V concluded the whole paper.

II. RELATED WORK

A. OVERVIEW OF VARICOSE VEINS OF THE LOWER EXTREMITIES

With the continuous advancement of society and the continuous improvement of living conditions, varicose veins have become a very common disease. In the early stage of human varicose veins, there is no change in the outer layer of the skin. In addition, people pay little attention to some diseases and are easily ignored by patients. Long-term occlusion of the lower extremity venous valve can cause veins. The backflow of blood causes blood to become silted, causing thrombosis, causing the disease to slowly increase, and finally causing the skin on the surface of the calf to slowly darken, followed by edema of the calf, thrombosis, and finally leg ulcers. If not

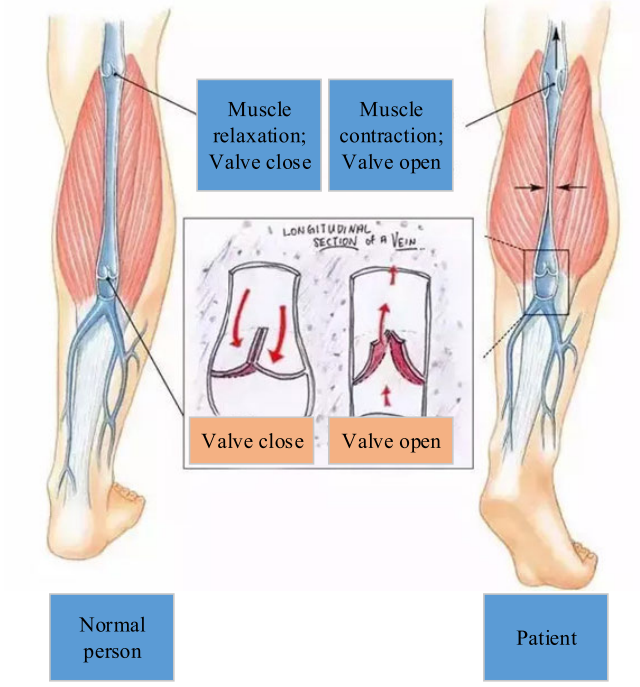

FIGURE 1. Comparison of varicose veins and normal veins.

treated in time, it may result in amputation or even formation. Thrombosis is life threatening and has a major impact on the lives and lives of patients. The comparison between varicose veins and normal veins is shown in Figure 1.

Lower extremity varicose veins are a common venous disease in vascular surgery, and the prevalence rate is the first in vascular disease [27]. Its clinical symptoms are eczema, pigmentation gradually worsening, lower extremity superficial vein dilatation, uplift, and distortion, easy to cause chronic ulcers, thrombophlebitis, and other complications, adversely affect the patient's labor and daily living ability.

Long-term continuous venous dilatation and blood reflux can lead to abnormal hemodynamics of lower limb veins, leading to hypoxia and the formation of chronic venous hypertension, leading to decreased blood flow shear force on the surface of vascular endothelial cells. Hypoxia, venous hypertension, and decreased sheer force of blood flow are important factors leading to the initiation of varicose venous inflammatory response. The study of Ijsselmuiden *et al.* [28] found that perfusion of hypoxic solution into the vein can cause adhesion reaction between neutrophils and endothelial cells, suggesting that a certain degree of decrease in blood oxygen partial pressure, such as during blood stasis, can cause activation of vascular endothelial cells. Moreover, the enhanced adhesion reaction between neutrophils and endothelial cells promoted the production of reactive oxide species (ROS) caused the release of multiple cytokines, leukotriene B4, and other inflammatory mediators. Prolonged hypoxia can induce the activation of hypoxia-inducible factor 1. Study found, in varicose vein organization, intercellular adhesion molecule -1 white blood cells and endothelial cells adhesion molecule 1 positive expression has the expression of HIF-1 alpha. Recent evidence suggests that hypoxia may activate ICAM-1 by directly activating the nuclear factor-kappa site on the promoter of the ICAM-1 gene, suggesting that hypoxia may increase the expression of ICAM-1 by activating nuclearfactor-κB. In addition, ICAM - 1 and vascular cell adhesion molecule – 1 in the resting on a low level expression of endothelial cells, the interferon - gamma and tumor necrosis factor alpha under the action of inflammatory cytokines, such as its expression can increase rapidly.

Studies have found that increased vascular tension and decreased blood flow shear force can act on vascular endothelial cells through a variety of signal transduction pathways, such as pro-cell mitotic protein kinase, produce ROS, and cause oxidative stress, resulting in endothelial cell damage and increased permeability. However, denaturation and shedding of endothelial cells in varicose veins were also found under electron microscope, which led to the loss of vascular endothelial cell barrier and the exposure of the underlying endothelial layer. Plasma levels of l-selectin and integrin CD11b on circulating neutrophils and monocytes decreased after standing for 30 min in a model of lower limb venous hypertension induced by CVD, suggesting that these inflammatory cells were trapped in microcirculation. Meanwhile, the level of soluble l-selectin in plasma increased, suggesting that these molecules shed from the surface of white blood cells during their adhesion to endothelial cells. Similar studies have found increased baseline levels of intercellular adhesion molecules icam-1, vcam-1, and elam-1 and von will brand factor in plasma of patients with varicose veins of the lower extremities, as well as those that reflect vascular endothelial cell injury. The evidence suggests in varicose veins when endothelial cells are activated or injured, it can produce and release a variety of cell-adhesion molecules that promote adhesion between endothelial cells and white blood cells, triggering an inflammatory response.

Inflammation of vascular endothelial cells is closely related to many cardiovascular and cerebrovascular diseases as well as peripheral vascular diseases, and is often an important link or an important manifestation of disease development. Varicose veins of the lower extremities are one of the most common vascular diseases, manifested as lower extremity swelling, superficial vein distorted dilatation, severe ulcer formation, local bleeding or infection [29]. It has been confirmed that there is a positive correlation between vascular endothelial cell inflammation and lower extremity varicose veins [30]. Therefore, this paper takes vascular endothelial cells as the research object, extracts the characteristics of cell images, and then classifies and recognizes varicose veins of lower extremities.

B. MULTISCALE IMAGE TECHNOLOGY

Multi-scale image technology is a method for multi-resolution expression of images. It refers to the technique of processing images at different scales after multi-scale segmentation.

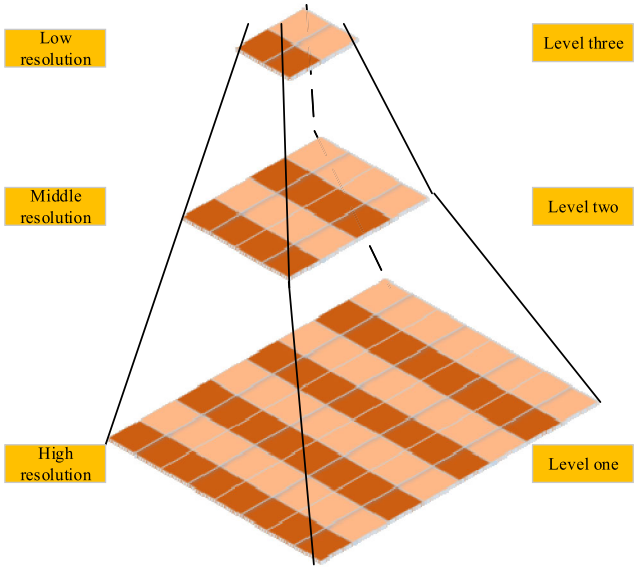

FIGURE 2. Image pyramid.

In many areas of visual image processing, it is not easy or difficult to extract complete features using a single scale. Therefore, this paper introduces multi-scale technology to assist feature extraction in feature extraction, so as to improve feature extraction ability. The implementation of multi-scale image technology, the primary task is to express the image under multi-scale conditions, to find the interconnection between the scales. Among them, the image pyramid is a typical multi-scale representation of images.

The image pyramid [31] is an analysis method based on multiple scales. It is essentially a layer-by-layer transformation resolution of the same image. A structure similar to a pyramid obtained by enlarging and reducing the image size is generally the bottom is a high-scale image and the upper part is a low-scale image. The image pyramid structure can represent images at different scales, similar to the human visual system, and describes the entire image in different scale spaces. In the process of image pyramid construction, down sampling is used. Therefore, when the image hierarchy is more, the image resolution is lower, and the resolution is worse, more image details are lost. However, images with smaller resolutions and sizes can exhibit more overall features, as shown in Figure 2. For example, after multi-scale treatment of vascular endothelial cell images, the lower the resolution of vascular endothelial cells, the smaller the size, the clearer the outline and detail of the vascular endothelial cells; the higher the resolution of vascular endothelial cells, the larger the size of the blood vessels size, and the more details of the endothelial cell image. In the image pyramid structure, extracting the features of multiple scale images can achieve the purpose of summarizing multiple scale information, and can improve the relevance and richness of feature expression. The following briefly introduces the type and construction of the image pyramid.

1) SUB-SAMPLING PYRAMID

The image pyramid can visually express the multi-scale structure. The general process of pyramiding an image is to use a low-pass filter for smoothing and down sampling the smoothed image. Among them, down sampling mainly extracts pixels from the horizontal and vertical directions of the image to reduce the image size, and the resolution of the adjacent two layers is reduced by a multiple of 2. According to the requirements of the scale space theory, the image size should be reduced while appropriate smoothing filtering. If the filter smoothing is not performed, the obtained pyramid is the sub-sampling pyramid. The sub-sampling pyramid is an effective down sampled representation of the image and is significantly effective in reducing image resolution. When creating a sub-sampling pyramid of an image, the pixels and the columns of the image are mainly sampled by pixels, and a thumbnail of the image size of 1/4 is obtained, and the sub-sampling process is repeated on the thumbnail until the constructed the number of image pyramid layers meets the experimental requirements.

When we construct the image pyramid, the size ratio of upper and lower images is always fixed at 1:4, and the image of the previous layer is obtained by down sampling the image of the latter layer. Therefore, the shape of the image pyramid has such a characteristic that the image resolution tends to gradually decrease from bottom to top, wherein the bottom is the original image, the top is the minimum resolution image, and the adjacent layer is down sampled, and the resolution is the layers differ by a factor of 1/4. In the image pyramid, the lower the resolution of the image, the clearer the image structure is. The more the bottom layer is, the higher the resolution of the image is, and the richer the image details of the local features of the image is.

2) GAUSSIAN PYRAMID

When constructing an image pyramid, a low-pass filter can be used for smoothing, depending on the type of filter used; different types of pyramids will be generated. For example, using a mean filter will generate a mean pyramid; using a Gaussian smoothing filter, a Gaussian pyramid will be generated. The choice of filter is related to the imaging quality of the subsampled image, and it is related to whether the pixel of the previous image can express the value of the next layer of the pixel value well. The core idea of the Gaussian pyramid is to use the original image as the bottom image, use Gaussian kernel convolution, then down sample the convolved image to get the previous image, and use the newly generated image as input again, repeat the convolution. In addition, the down sampling operation, after repeated iterations multiple times, forms a data structure.

The Gaussian function expression is

$$g(x) = \frac{1}{\sqrt{2\pi}\sigma} e^{-(x^2/2\sigma^2)} \tag{1}$$

Variable σ is the standard deviation and the smoothness of the signal is adjusted by this value. After discretizing the

Gaussian function, a Gaussian kernel for convolution can be obtained, taking the Gaussian kernel 5 × 5 as an example, and its expression is:

$$w = \frac{1}{256}\begin{bmatrix} 1 & 4 & 6 & 4 & 1 \\ 4 & 16 & 24 & 16 & 4 \\ 6 & 24 & 36 & 24 & 6 \\ 4 & 16 & 24 & 16 & 4 \\ 1 & 4 & 6 & 4 & 1 \end{bmatrix} \tag{2}$$

3) GAUSSIAN DIFFERENCE PYRAMID

The difference of Gaussian is actually an approximation to the Laplace of Gaussian (LoG), which is the difference between two Gaussian functions with different variances and is a band pass filter. The filter function expression is

$$\begin{aligned} D(x, y, \sigma_1, \sigma_2) &= (G(x, y, \sigma_1) - G(x, y, \sigma_2)) * I(x, y) \\ &= L(x, y, \sigma_1) - L(x, y, \sigma_2) \end{aligned} \tag{3}$$

Variable $I(x, y)$ is the original image, $G(x, y, \sigma_1)$ is a Gaussian function with a distribution parameter of σ_1, $G(x, y, \sigma_2)$ is a Gaussian function with a distribution parameter of σ_2, and $*$ represents a volume product.

Therefore, the response image of dog is $D(x, y, \sigma_1, \sigma_2)$, and it is essentially the difference between two different Gaussian smoothed images, namely $L(x, y, \sigma_1) - L(x, y, \sigma_2)$. The filter is band-passable, so it can better reflect the visual characteristics of the image, and it is widely used in edge detection.

C. DEEP CONVOLUTIONAL NEURAL NETWORK

Deep learning is relative to the shallow learning model. In a narrow sense, it is a multi-layer neural network model with multiple hidden layers, with specific structure and training methods. The idea of deep learning is based on the visual mechanism of the human brain. In 1981, Nobel Prize winners David Hubei discovered that the information processing of the human brain's visual system is hierarchical, from the pupil's original pixel that is the cerebral cortex. Some cells do preliminary processing, such as finding edge information of the input signal. Then the brain abstracts the entire input pixel information according to the edge information, and further determines other shapes such as the shape of the object formed by the pixel information. Upon completion, the cerebral cortex will perform a higher level of abstraction of the information obtained, and then it can be determined what the object in front of it is. Deep learning is to learn from this process, to realize the modeling of this process through computer, starting from the original input image, through the unsupervised training of multi-layer structure, abstracting and learning the image features layer by layer, and the whole network can be utilized.

Deep learning is based on artificial neural theory. By optimizing the learning algorithm, compared with the traditional neural network, it focuses on the nonlinear transformation of features, has more network structure levels, and can express more abstract features of images. The field of machine vision such as image classification and recognition has been widely used and it achieved very significant recognition effects. Because deep learning technology has good nonlinear fitting ability, and has made major breakthroughs in image classification, recommendation system, target detection and tracking, computational advertising, image segmentation, quantitative investment, speech recognition, etc., making deep learning technology become The research focus of various universities, research institutes and companies. Deep learning can learn high-level abstract features from low-level features such as pixels of images, which can be applied to many areas where traditional artificial intelligence technology is not suitable.

Deep learning follows online learning methods, including supervised learning and unsupervised learning. Among them, supervised learning is represented by deep convolutional neural network [32], [33], which has end-to-end learning ability and good classification and prediction performance. Unsupervised learning is represented by automatic encoder and can reconstruct original input image. The network middle layer is used as a feature representation of the image. The unsupervised deep learning network can use the self-learning function to pre-train the network with a large number of images unrelated to the research topic, and then fine-tune the classified data, which can be widely used in the research field of insufficient tag data.

At present, benefiting from the development of computer hardware and big data networks, the Internet and social media provide a large amount of available image resources, which has led to the development of research based on supervised deep learning. Among them, the study of deep convolutional neural networks is the most concerned. At present, a large number of deep convolutional neural network models are trained on a database scale of more than one million, and have good network generalization performance, which fully reflects the classification and discriminative performance of deep convolutional neural networks.

1) CONVOLUTIONAL NEURAL NETWORK STRUCTURE

The most representative network structure in deep learning is Convolutional Neural Networks (CNN). In addition, it has achieved great success in several fields, such as machine vision. Compared with traditional image processing algorithms, CNN has the advantage of using the end-to-end learning ability to directly use the original image as input, without excessive manual intervention, and avoiding pre-processing of the image. Compared with the traditional neural network, CNN has the advantages of adopting the local connection structure and having the characteristics of simple model construction. Moreover, the weight sharing mechanism between the neurons is used, so that the weight parameter to be trained is the size of the convolution kernel. Not related to the number of hidden layer neurons, further reducing the trainable parameters. Although the weight parameters have been greatly reduced, the CNN network still exhibits excellent feature extraction capabilities.

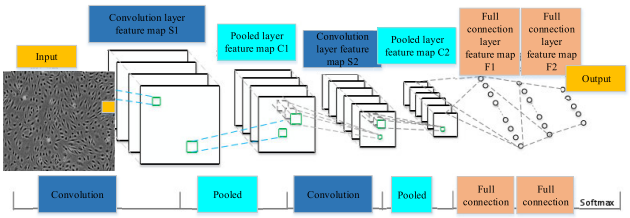

FIGURE 3. Convolutional neural network structure.

In the Convolution Layer, each node is only partially connected to an adjacent network layer. A convolution kernel can extract a feature. By adding more convolution kernels, more features can be obtained. This feature obtained by convolution kernel mapping is called a feature map. Each layer generally contains a number of feature maps. Each feature map is composed of a plurality of square-arranged nodes. The nodes of the same feature plane adopt the same weight parameter, that is, the shared weight. In the process of training, the convolution kernel usually uses a matrix consisting of small values to perform random initialization. Through continuous learning, the final training gets the appropriate weight. Each convolution kernel share weight can reduce the connection between adjacent network layers and it can reduce the likelihood of convolutional neural networks over-fitting on the training set. The pooling layer is also known as the down sampling layer. It generally includes two methods of max pooling and means pooling. The former is in practice. There are relatively many applications. The convolutional and pooling layers of the convolutional neural network can greatly reduce the complexity of the network and significantly reduce the parameters of the network.

The convolutional neural network consists of two parts: feature extraction and feature mapping, including convolution, activation and pooling. Finally, it is classified in the softmax classifier. A typical CNN structure consists of an image input layer, a convolution layer, an activation layer, a pooling layer, a fully connected layer, and a softmax classifier, as shown in Figure 3.

2) CONVOLUTIONAL LAYER

The convolutional layer of the convolutional neural network limits the connection between the implicit unit and the input unit by local sensing, so that each implicit unit can only connect a small portion of the adjacent area of the input image. The weight parameter of the convolutional layer is mainly a series of convolution kernels. A convolution check performs a bulk convolution operation on the entire image, extracts a feature map. The operation of the convolution kernel is:

$$S(i,j) = (X * W)(i,j) + b = \sum_{k=1}^{M} (X_k + W_k)(i,j) + b \quad (4)$$

The variable M means the number of input images, X_k is the k-th input image, W_k is the kth sub-convolution kernel of the convolution kernel. The variable b is the offset. S is

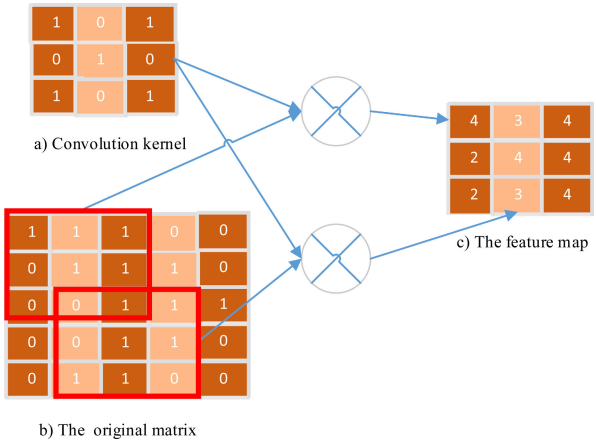

FIGURE 4. Schematic diagram of convolution operation.

feature map corresponding to the convolution kernel W, and $S(i, j)$ means the value of the corresponding position element in the feature map corresponding to the convolution kernel W. Taking the 5×5 input matrix, a 3×3 convolution kernel, and a convolution step as one pixel; the convolution process is shown in Figure 4.

3) ACTIVATION FUNCTION

The activation function mainly provides non-linear expression ability for convolutional neural networks to solve the problem of linear indivisibility. The activation function is an indispensable part of the convolutional neural network; if there is no activation function, the network can only perform linear mapping, even if the network hierarchy is equivalent to a single-layer network. At present, there are two main types of activation functions, which are piecewise linear and nonlinear functions with exponential shapes.

The sigmoid function, which has an exponential function shape, is the most widely used type of activation function, and its function expression is

$$f(x) = 1/(1 + e^{-x}) \quad (5)$$

Among them, the sigmoid function has a value range of (0, 1) and has a monotonous increment, which can be used for probability or input normalization. The most obvious defect of the sigmoid function is soft saturation, that is, the derivatives on both sides of the function gradually approach zero, that is,

$$\lim_{x->\infty} f'(x) = 0 \quad (6)$$

This soft saturation of the sigmoid function has a gradient dispersion problem, making deeper neural networks less prone to training and limiting the application of neural networks.

The Tanh function (hyperbolic tangent) is another common exponential shape activation function with a range of $[-1, 1]$ and a function expression of

$$f(x) = (1 - e^{-2x})/(1 + e^{-2x}) \quad (7)$$

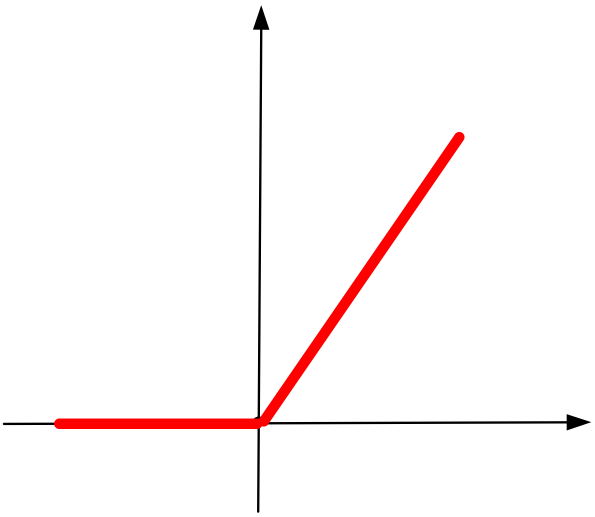

FIGURE 5. ReLU activation function.

Similar to the sigmoid function, the Tanh function also has soft saturation, which is easy to cause gradient dispersion, but this function has faster convergence speed than the sigmoid function.

The ReLU linear correction unit is a piecewise linear function whose function is expressed as

$$f(x) = \max(x, 0) \tag{8}$$

The graph of the ReLU activation function is shown in Figure 5. When x>0, ReLU can maintain the gradient without attenuation, which can alleviate the gradient dispersion problem, making it possible to train the deep network directly in a supervised manner.

4) POOLING LAYER

The essence of the pooling layer is sampling. For the input feature map, it is compressed in some way, and the main parameters of the image are extracted while reducing the network parameters, so that it is more capable of characterizing. At the same time, the reduction of network parameters is also beneficial to prevent over-fitting.

There are two commonly used pooling methods: mean-pooling and max-pooling. Take the 2 × 2 maximum pooling with a step size of two pixels as an example, as shown in Figure 6 and Figure 7. Among them, only one of the maximum value pooled convolution kernel weight values is 1, and the rest is 0. The convolution kernel is the location where 1 corresponds to the maximum value of the element in the feature map where the convolution kernel is placed.

The convolution kernel slides in the feature map in two pixel steps. After the maximum value is sampled, the feature map is reduced to the original 1/4. The average pooling is similar to the implementation of the maximum sampling, except that the average of the elements of the coverage area of the feature map is extracted and used as the output. The size of the final output map is related to the sliding step size

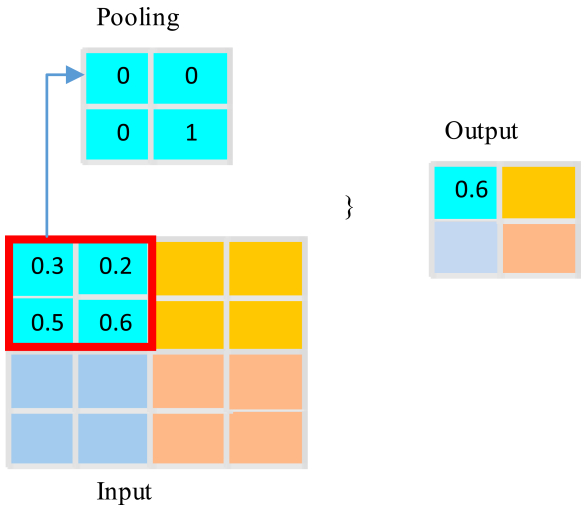

FIGURE 6. Max Pooling.

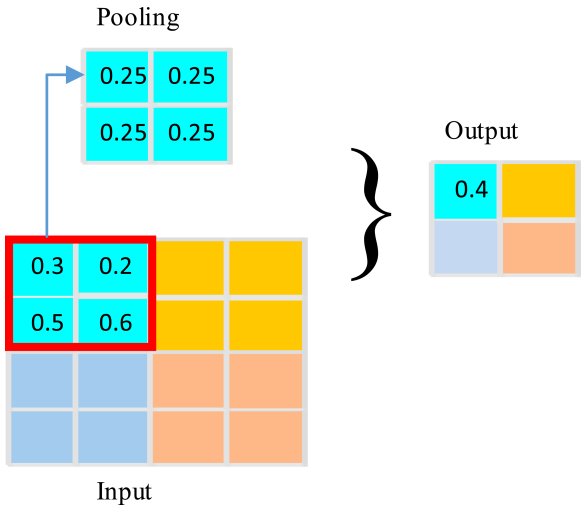

FIGURE 7. Mean Pooling.

of the convolution kernel. Taking two pixels as an example, the output feature map is 1/4 of the original image.

III. MULTI-SCALE DEEP LEARNING NETWORK

Researchers, and a series of research results have been produced, which has greatly promoted the research progress of medical images, have favored the application of deep convolutional neural networks in medical images. However, due to the lack of open large-scale databases, most of the research using deep convolutional neural networks is carried out on self-built small-scale databases, and the robustness of the network is not very good. Moreover, deep convolutional neural networks use supervised training methods. In order to improve the generalization performance of the network, it is necessary to deepen the network hierarchy or seek a more reasonable network structure. As the network level deepens, more tagged training data is needed for fitting. Therefore, it is necessary to accurately design the network structure while taking into account the size of the network.

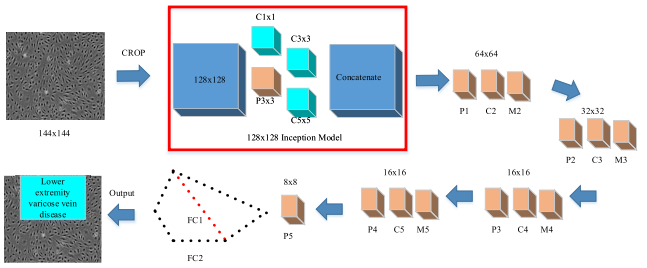

FIGURE 8. Lightweight deep convolutional neural network with enhanced feature extraction.

In view of the above analysis, a lightweight deep convolutional neural network for the study of enhanced feature extraction of vascular endothelial cells was constructed. On the one hand, large-scale database training, large-scale database not only has a large number of sample images, but also contains more shape images, through a large number of labeled images, can extract more complete image features, improve network generalization performance. In terms of multi-scale image technology, the feature extraction capability of network is improved. In addition, the Max-Feature-Max (MFM) activation layer [34] is used instead of the Rectified Linear Units activation layer to introduce a competition mechanism and reduce the network. The weighting parameters can be trained to streamline the network structure.

This paper combines the network structure features of Google-Net, VGG and literature [35] to construct a lightweight deep convolutional neural network with enhanced feature extraction, as shown in Figure 8. The letter "C" indicates the base layer of the volume. "M" indicates the MFM activation layer. "P" indicates max pooling, and "Fc" indicates fully connected layer. In Figure 8, the first convolutional layer uses the Inception Model, which is based on the "split-merge" strategy, which extracts multi-scale features of the image through multiple convolutional layers, and has the function of enhancing feature extraction. The discriminative features of vascular endothelial cell images include not only the overall features but also the local features. Different scale images reflect different spatial information relationships, and extract features from multiple scales, which can include more abundant classification features. The MFM activation layer follows the 2nd to 5th convolutional layers. The competitive mechanism introduced by the MFM activation layer can make the network features more compact, further reduce network parameters, and improve network operation speed. Layers 6 through 7 are fully connected layers, and the final extracted 256-dimensional features are used to represent the output of the five categories. Literature [36] shows that smaller convolution kernels can improve predictions. Therefore, the network constructed in this chapter uses a convolution kernel with a fixed size of 3 × 3, and uses the literature [37] to construct a deep network, using a 1 × 1 convolution layer to simplify the network weight parameters, and the network training constructed. The parameter is 5650K for small-embedded devices.

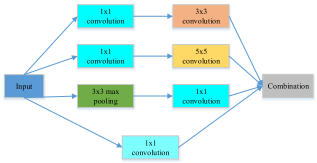

FIGURE 9. Inception Model unit structure.

A. INCEPTION MODEL

Google-Net uses the inception model as the foundation unit of the network structure. The unit extracts different scale features of the image with convolution kernels of different sizes, which can enhance feature extraction. The Inception model increases the width of the hidden layer. The addition of hidden layers can extract more features and improve network prediction. The inception model structure is shown in Figure 9. The model consists of many layers, the number of 1×1 convolutional layers is four, the number of 3×3 convolutional layer is one, the number of 5×5 convolutional layer also is one, and the number of 3×3 down sampling layer is one. The use of convolution kernels of different sizes can obtain different scale image features of different scales, thereby enhancing the feature extraction capability of the inception model. Among them, 1×1 convolution kernel is used for dimensionality reduction. Set the PAD value to 0, 1, and 2 in the network to output the same dimensions in the merge layer. In this paper, only one inception model is placed after the data layer. The other layers use the traditional convolution layer and MFM activation function.

B. ACTIVATION FUNCTION

The activation functions used by convolutional neural networks are mainly ReLU and MFM. Like a linear activation function, ReLU is easy to optimize and outputs zero on a domain with an input value less than zero. With one-sided activation and forced sparsity, which makes the ReLU activation function active, its derivative can maintain a large value, effectively solving the gradient disappearance problem and improving the network convergence speed.

Since the ReLU activation function only performs a simple linear transformation, the nonlinear representation ability is low. In literature [37], by modifying the max out activation function, an MFM activation function is proposed, which has the function of making features compact and reducing parameters. Relative to ReLU forced dilution; it retains the maximum information of the feature through a competitive mechanism, as shown in Figure 10.

Suppose there are 2N convolutional layer outputs, $X^n \in R^{H \times W}$, $n \leq 2N$ and then the implementation formula of the MFM activation function, i.e.

$$f_{ij}^k = \max(X_{i,j}^k, X_{ij}^{k+m}) \tag{9}$$

where X is the feature layer of the convolution output, $1 \leq i \leq h, 1 \leq j \leq w$ and the implementation principle is shown in Figure 10. The gradient of equation (9) is calculated

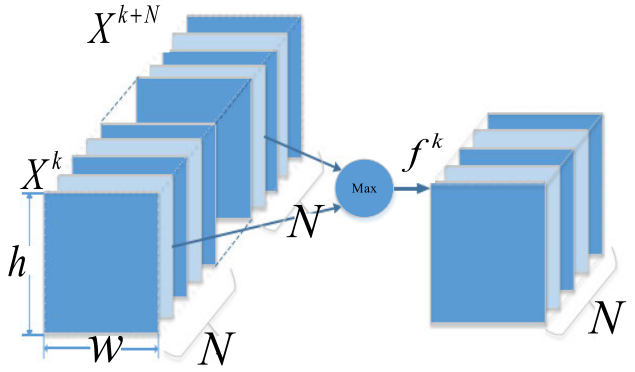

FIGURE 10. MFM activation function implementation schematic.

as equation (10) and equation (11).

$$\frac{\partial f}{\partial X^{k'}} = \begin{cases} 1, & X_{i,j}^{k} \geq X_{ij}^{k+n} \\ 0, & else \end{cases}, \quad 1 \leq k' \leq 2n \tag{10}$$

$$k = \begin{cases} k', & 1 \leq k' \leq n \\ k' - n, & n+1 \leq k' \leq 2n \end{cases} \tag{11}$$

C. DEPTH SEPARABLE CONVOLUTION

This paper introduces a deep separable convolution model, which is composed of channel convolution and point convolution, which can improve the efficiency of convolution operation. It can be effectively solved by splitting ordinary convolution operations and performing point-by-point convolution. Reduce the amount of convolution operations. The depth separable convolution is based on the ordinary convolutional layer, referencing the packet convolution strategy, and from the multidimensional space perspective, independent convolution between different groups of input feature maps. If input the feature map of the end is divided into Group = S group, then the feature map of each M/S group input constitutes a convolution subset, and the convolution strategy convolution of common convolution layer shared weights is used to obtain an output feature map. The feature maps are grouped by depth, and then the input feature map and the output feature map can be concatenated one-to-one. After the point-by-point convolution, 1 × 1 convolution is performed to realize the fusion of the channel-by-channel convolution map and map the feature map to new channel space.

D. MULTI-SCALE DEEP LEARNING NETWORK STRUCTURE

The multi-scale deep learning network constructed in this paper consists of an inception model, four 3 × 3 convolutional layers, four 1 × 1 convolution kernels, nine MFM activation layers and two fully connected layers. The network integrates Google-Net and literature [37] Network structure characteristics. The detailed structure configuration is shown in Table 1.

The image size is 144 × 144. After inputting the model, it is randomly cut into 128 × 128 size to increase the amount of data. After each pooling layer, the 1 × 1 convolutional layer and the MFM activation function are used for dimensioning and dimensionality reduction. A pooling layer follows each 3 × 3 convolution layer. These two parts form a unit and are repeated. Stacking increases the depth of the network. The MFM activation function and the Dropout layer for dimensionality reduction to prevent overfitting follow the first fully linked layer.

TABLE 1. Deep convolutional neural network configuration.

Types	Filter /stride pad	Feature size	Parameter
Input	-	144×144×1	-
Crop	-	128×128×1	-
Inception	-	128×128×256	159K
Pool1	-	64×64×256	-
Conv2a	1×1/1	64×64×96	24K
MFM2a	-	64×64×48	-
Conv2	3×3/1,1	64×64×192	83K
MFM2	-	64×64×96	-
Pool2	2×2/2	32×32×96	-
Conv3a	1×1/1	32×32×192	18K
MFM3a	-	32×32×96	-
Conv3	3×3/1,1	32×32×384	331K
MFM3	-	32×32×192	-
Pool3	-	16×16×192	-
Conv4a	1×1/1	16×16×384	73K
MFM4a	-	16×16×192	-
Conv4	3×3/1,1	16×16×256	442K
MFM4	-	16×16×128	-
Conv5a	1×1/1	16×16×256	32K
MFM5a	-	16×16×128	-
Conv5	3×3/1,1	16×16×256	294K
MFM5	-	16×16×128	-
Pool4	2×2/2	8×8×128	-
Fc1	-	512	4194K
MFM_Fc1	-	256	-
Fc2	-	5	-
Total	-	-	5650K

The operation steps of the algorithm are as follows:

(1) This paper preprocesses the acquired images. Before network training, a series of preprocessing processes such as clipping are carried out on the images in the database, and the images are converted into images with the same scale and size to adapt to network training.

(2) Due to the deviation and tilt of the images of vascular endothelial cells in the original database, it is necessary to take such operations as alignment of the images of vascular endothelial cells.

(3) Send the processed image to the network for training. When the loss function is converged, the training stops.

(4) Preprocess the collected test images, and apply the weight and other parameters generated by training into the test images.

IV. ANALYSIS OF RESULTS

A. DATA ACQUISITION DEVICE

The Internet of Things refers to the connection of any object to the network through the information-sensing device

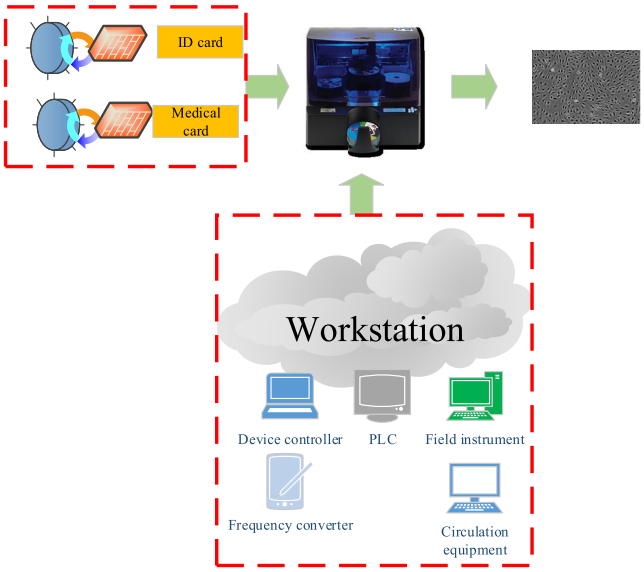

FIGURE 11. Image acquisition device combining internet of things and medical device.

according to the agreed protocol. The object exchanges information and communicates through the information media to realize intelligent identification, positioning, tracking, and supervision. In the 21st century, the Internet of Things technology and related industries have developed rapidly. More and more mobile terminals use Internet of Things technology to achieve intelligent identification. In this paper, through the using of Internet of Things technology and medical knowledge, a device that combines Internet of Things technology with medical images is designed. Through the sensor network of the Internet of Things technology, the required information can be collected, and the collected multi-source information and the mobile device can be combined to realize the acquisition of the medical image, as shown in Figure 11.

B. IMAGE PREPROCESSING

Because the size and resolution of vascular endothelial cells are not uniform in the database, if the original image is not preprocessed, the effect of network training and the robustness of the network are reduced. Therefore, this paper preprocesses the acquired image. Before performing network training, a series of preprocessing processes such as cropping the image in the database are first performed, and the image is converted into an image with the same scaling and size to adapt to network training.

Due to problems such as deflection and tilt of the vascular endothelial cell image in the original database, it is necessary to perform alignment and the like on the vascular endothelial cell image.

Finally, the image scaling method is used to scale the image, and three levels of processing are performed to obtain three data sets of different resolutions and sizes, as shown in Figure 12.

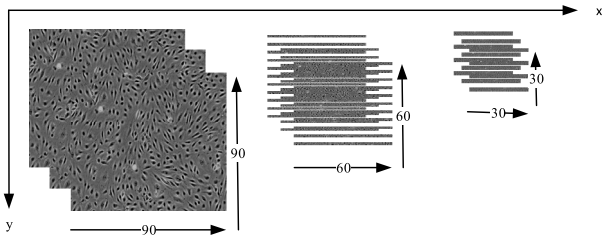

FIGURE 12. Multi-scale training set.

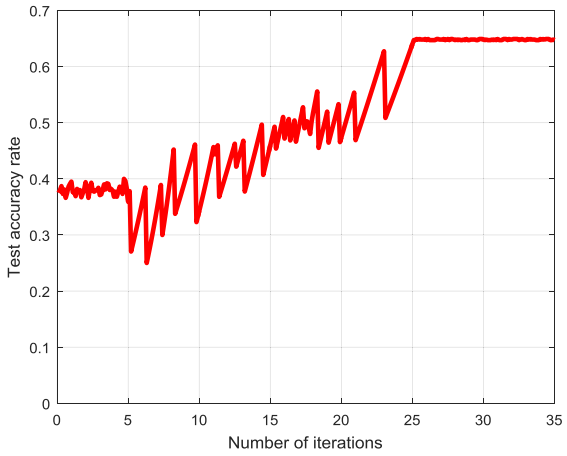

FIGURE 13. Testing accuracy of the MSDCNN model.

C. NETWORK TRAINING CORRECT RATE AND LOSS CURVE

The testing accuracy and loss and training curves of the MSDCNN model by maximum pooled down sampling mode are shown in Figure 13, Figure 14, and Figure 15. The training network tends to converge after 300,000 iterations, achieving the highest test accuracy.

It can be seen from Figure 13, Figure 14, and Figure 15 that with the increase of the number of network iterations, the test accuracy rate gradually increases and tends to be stable; the test loss gradually decreases and tends to be stable; when iteration is 300,000 times, the network gradually converges. At the same time, the network training loss is gradually shrinking. This result shows that the network designed by us can run normally on the database.

D. NETWORK PERFORMANCE COMPARISON

This paper divides 10000 images into training set and test set proportionally. Among them, the training set accounts for 80% and the test set accounts for 20%. The hyper-parameter settings for MSDCNN training are shown in Table 2.

The initial learning rate learning_rate_p is set to 0.0005, the momentum_p is set to 0.9, the weight_decay_p is set to 0.005, the learning strategy is set to fixed mode fixed, and the maximum number of iterations max_iter_p is set to 700,000 times. When the training accuracy rates no longer increases and the maximum correct value attachment changes, the learning rate is reduced and training continues until the correct rate no longer increases. To prevent overfitting from occurring, the dropout layer follows the fc1 full-link

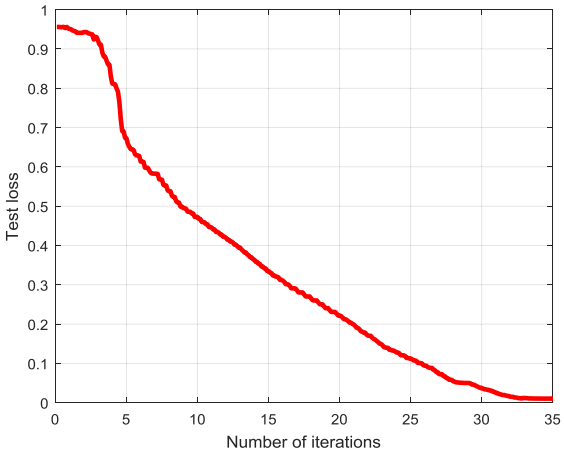

FIGURE 14. The testing loss curve of the MSDCNN model.

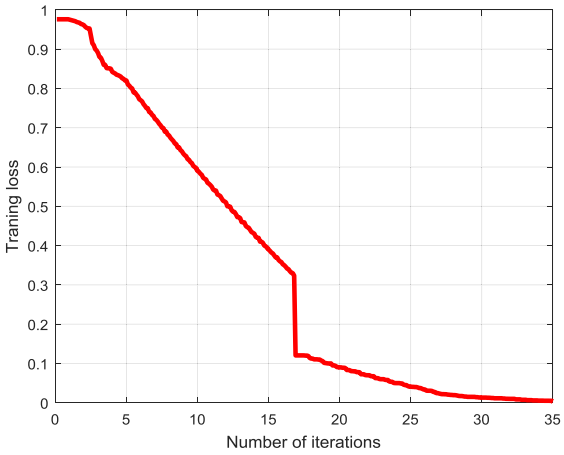

FIGURE 15. The training loss curve of the MSDCNN model.

TABLE 2. The value of training hyper-parameters.

Hyper-parameters	Value
learning_rate_p	0.0005
momentum_p	0.9
weight_decay_p	0.0005
learning_rate _policy_p	fixed
power_p	0.75
max_iter_p	700000

layer MFM activation function, and the parameter power_p is set to 0.75. The initial weight of the convolution filter is initialized with the offset is fixed at 0.1.

In order to illustrate the effectiveness of the proposed model, this paper uses the traditional method to conduct experiments on the database. The SVM classifier is used as the training model, and the rank-1 statistical correct rate is used. The test results are shown in Table 3. The features used for classification were LPQ, LBP, Raw Pixel, K-means, and Multi-scale k-means (MSK). As can be seen from the results in Table 3, compared with the classification effect of traditional learning methods, the method based on deep learning has a good classification effect.

TABLE 3. Deep learning and traditional learning method test results.

Index		Rank-1
Featur e	LBQ	0.386
	LBP	0.421
	Raw Pixel	0.468
	K-means	0.507
	MSK	0.527
	MSDCNN	0.623

TABLE 4. Test results of deep learning and traditional learning methods (data enhancement).

Index		Rank-1
Feature	LBQ	0.433
	LBP	0.437
	Raw Pixel	0.498
	K-means	0.533
	MSK	0.565
	MSDCNN	0.635

TABLE 5. Test results of multiple deep neural network models.

Network model	Rank-1
NIN [38]	0.573
DeepID2 [39]	0.578
Google-Net [40]	0.591
VGG_CNN_S [41]	0.596
MSDCNN	0.635

Due to the lack of an open database, the performance of the proposed model algorithm cannot be verified on other databases. Therefore, this paper uses the data enhancement processing method to process the database and retrain the traditional classifier and MSDCNN model. The prediction results based on the traditional learning method are shown in Table 4. After increasing the image size of the training set, the classification accuracy rate of the traditional learning method is improved. Among them, the MSK method achieved a correct classification rate of 56.5%. The classification accuracy of MSDCNN constructed in this paper is 63.5%.

The classification accuracy and running time based on the deep learning method are shown in Table 5 and Table 6. With the increase of training set size, the correct classification rate of MSDCNN is improved, and the running time is the least. Experiments show that the classification effect of deep learning is better than that of traditional learning methods, and deep learning requires many tags to fit. Therefore, one way to improve the classification performance of the network is to increase the amount of data.

E. NETWORK EFFICIENCY AND PARAMETER QUANTITY

The MSDCNN model network training parameter quantity is related to the network depth and the number of network filters in each layer. The deeper network layer and wider

TABLE 6. Running time of multiple deep neural network models for single image acquisition.

Network model	Time/ms
NIN [38]	773
DeepID2 [39]	898
Google-Net [40]	791
VGG_CNN_S [41]	981
MSDCNN	521

TABLE 7. Network training parameters of multiple deep neural network models.

Model	Structure	Parameter /k
NIN [38]	3 common volume base layers, 6 1×1 convolution layers	2 348
Google-Net[40]	10 inception modules	6 797.7
VGG_CNN_S[41]	5 common volume base layers, 2 full connection layers	25 392
MSDCNN	7 1×1 convolution layers, 7 separable convolution layers	683.7

network width can extract more abundant network features and improve the network's feature representation ability. Table 6 gives 4 the statistical value of the training parameter quantity of the deep convolutional neural network model, wherein the VGG_CNN_S has the largest amount of trainable parameters, but the network training has higher hardware requirements and longer time consumption. The network parameters of NIN and Google-Net are smaller than VGG. The network training time is shorter, the resource overhead is smaller, and the network execution efficiency is higher. At the same time, the MSDCNN model constructed in this paper introduces the deep separable convolution layer, the model parameter calculation amount is the smallest, and the network runs fastest, not only in the network. The desktop computer with graphics card can run fast, and it can be quickly run on the portable mobile device. Combined with image multi-scale technology, it can still achieve high classification accuracy while reducing the parameters of deep convolutional neural network model.

V. CONCLUSION

There is a positive correlation between vascular endothelial cell inflammation and varicose veins of the lower extremities. Therefore, this paper uses vascular endothelial cells as the research object to construct a deep convolutional neural network for varicose veins of lower extremities to improve the accuracy of classification and recognition. The network uses Google-Net's inception model as the first convolutional layer to process the data layer, and extracts multi-scale features of the image through multiple convolutional layers to enhance the feature extraction capabilities of the network. At the same time, the MFM activation function is used instead of the ReLU activation function to introduce a competition mechanism, which can extract features that are more compact and reduce network layer parameters, which is used to improve network feature extraction capability. Compared with the existing deep convolutional neural network model, the network can improve the feature extraction capability of the network, has the characteristics of fast running speed, few network parameters, and is suitable for small-embedded devices. Although this paper has obtained relatively good experimental results, there are still many problems when it is applied to clinical practice only under the experimental environment. Improving the network and applying it to clinical practice is what we need to do next.

REFERENCES

[1] H. Lau, J. Chang, N. Daut, A. Tahir, E. Samino, and M. H. Hijazi, "Exploring edge-based segmentation towards automated skin lesion diagnosi," *Adv. Sci. Lett.*, vol. 24, no. 2, pp. 1095–1099, 2018.

[2] E. S. Asl, M. Ghazal, A. Mahmoud, A. Aslantas, A. Shalaby, M. Casanova, G. Barnes, G. Gimel'Farb, R. Keynton, and A. El Baz, "Alzheimer's disease diagnostics by a 3D deeply supervised adaptable convolutional network," *Frontiers Biosci.*, vol. 23, no. 2, pp. 584–596, 2018.

[3] J. Kawahara, C. J. Brown, S. P. Miller, B. G. Booth, V. Chau, R. E. Grunau, J. G. Zwicker, and G. Hamarneh, "BrainNetCNN: Convolutional neural networks for brain networks; Towards predicting neurodevelopment," *NeuroImage*, vol. 146, pp. 1038–1049, Feb. 2017.

[4] W. Shen, M. Zhou, F. Yang, C. Yang, and J. Tian, "Multi-scale convolutional neural networks for lung nodule classification," in *Information Processing in Medical Imaging*, vol. 24. Cham, Switzerland: Springer, 2015, pp. 588–599.

[5] Y. Yuan, M. Chao, and Y.-C. Lo, "Automatic skin lesion segmentation using deep fully convolutional networks with Jaccard distancw," *IEEE Trans. Med. Imag.*, vol. 36, no. 9, pp. 1876–1886, Sep. 2017.

[6] M. A. Al-Antari, M. A. Al-Masni, M.-T. Choi, S.-M. Han, and T.-S. Kim, "A fully integrated computer-aided diagnosis system for digital X-ray mammograms via deep learning detection, segmentation, and classification," *Int. J. Med. Inform.*, vol. 117, pp. 44–54, Sep. 2018.

[7] J. Xu, L. Xiang, Q. Liu, H. Gilmore, J. Wu, J. Tang, and A. Madabhushi, "Stacked sparse autoencoder (SSAE) for nuclei detection on breast cancer histopathology images," *IEEE Trans. Med. Imag.*, vol. 35, no. 1, pp. 119–130, Jan. 2016.

[8] J. Shi, Y. Qian, J. Wu, S. Zhou, Y. Cai, Q. Zhang, X. Feng, and C. Chang, "Ultrasound image based tumor classification via deep polynomial network and multiple kernel learning," *Current Med. Imag. Rev.*, vol. 14, no. 2, pp. 301–308, 2018.

[9] M. A. Moreno-Eutimio, L. Espinosa-Monroy, T. Orozco-Amaro, Y. Torres-Ramos, A. Montoya-Estrada, J. J. Hicks, E. Rodriguez, P. Del Moral, J. Moreno, and J. Cueto, "Enhanced healing and anti-inflammatory effects of a carbohydrate polymer with zinc oxide in patients with chronic venous leg ulcers: Preliminary results," *Arch. Med. Sci.*, vol. 14, no. 2, pp. 336–344, 2018.

[10] Y. Kinomura, T. Tanaka, T. Aoyama, M. Hatasa, S. Minatoguchi, M. Iwasa, Y. Yamada, T. Nawa, H. Kanamori, M. Kawasaki, Y. Esaka, B. Uno, K. Nishigaki, and S. Minatoguchi, "Endogenous adenosine may be related to left ventricular dysfunction, dilation, and wall thinning in patients with heart disease," *Circulat. J.*, vol. 82, no. 5, pp. 1319–1326, 2018.

[11] C. Ferraresi, C. De Benedictis, D. Maffiodo, W. Franco, A. Messere, R. Pertusio, and S. Roatta, "Design and simulation of a novel pneumotronic system aimed to the investigation of vascular phenomena induced by limb compression," *J. Bionic Eng.*, vol. 16, no. 3, pp. 550–562, 2019.
[12] B. Kozma, K. Candiotti, R. PóKa, and P. Takács, "The effects of heat exposure on vaginal smooth muscle cells: Elastin and collagen production," *Gynecologic Obstetric Invest.*, vol. 83, no. 3, pp. 247–251, 2018.
[13] P. Gloviczki, A. J. Comerota, M. C. Dalsing, B. G. Eklof, D. L. Gillespie, M. L. Gloviczki, J. M. Lohr, R. B. McLafferty, M. H. Meissner, M. H. Murad, F. T. Padberg, P. J. Pappas, M. A. Passman, J. D. Raffetto, M. A. Vasquez, and T. W. Wakefield, "The care of patients with varicose veins and associated chronic venous diseases: Clinical practice guidelines of the society for vascular surgery and the American venous forum," *J. Vascular Surg.*, vol. 53, no. 5, pp. 2S–48S, 2011.
[14] H. J. Welch, L. Kabnick, M. A. Vasquez, D. L. Monahan, F. Lurie, and G. Jacobowitz, "Proposal for a national coverage determination for the treatment of varicose veins and venous disease due to disparate centers for medicare and medicaid services local coverage determination policies," *J. Vascular Surg., Venous Lymphatic Disorders*, vol. 5, no. 3, pp. 453–459, 2017.
[15] E. L. Chaikof, R. L. Dalman, M. K. Eskandari, B. M. Jackson, W. A. Lee, M. A. Mansour, T. M. Mastracci, M. Mell, M. H. Murad, L. L. Nguyen, G. S. Oderich, M. S. Patel, M. L. Schermerhorn, and B. W. Starnes, "The society for vascular surgery practice guidelines on the care of patients with an abdominal aortic aneurysm," *J. Vascular Surg.*, vol. 67, no. 1, p. 2-77.e2, 2018.
[16] B. Santler and T. Goerge, "Chronic venous insufficiency—A review of pathophysiology, diagnosis, and treatment," *J. Deutschen Dermatologischen Gesellschaft*, vol. 15, no. 5, pp. 538–556, 2017.
[17] O. Nelzén and I. Fransson, "Varicose vein recurrence and patient satisfaction 10–14 years following combined superficial and perforator vein surgery: A prospective case study," *Eur. J. Vascular Endovascular Surg.*, vol. 46, no. 3, pp. 372–377, 2013.
[18] P. A. Patel, A. M. Barnacle, S. Stuart, J. G. Amaral, and P. R. John, "Endovenous laser ablation therapy in children: Applications and outcomes," *Pediatric Radiol.*, vol. 47, no. 10, pp. 1353–1363, 2017.
[19] Y. Liu, Y. M. Li, W. B. Yang, and G. Cao, "Endovenous laser ablation versus conventional surgery for great saphenous varicose veins: Meta-analysis of randomized trials," *Zhonghua Yi Xue Za Zhi*, vol. 93, no. 23, pp. 1822–1826, 2013.
[20] G. D. Baxter, L. Liu, S. Tumilty, S. Petrich, C. Chapple, and J. J. Anders, "Low level laser therapy for the management of breast cancer-related lymphedema: A randomized controlled feasibility study," *Lasers Surg. Med.*, vol. 50, no. 9, pp. 924–932, 2018.
[21] E. DePopas and M. Brown, "Varicose veins and lower extremity venous insufficiency," *Seminars Intervent. Radiol.*, vol. 35, no. 1, pp. 56–61, 2018.
[22] Y. Chen, J. Wang, X. Zhu, X. Chen, X. Yang, K. Zhang, Y. Fan, and X. Zhang, "The directional migration and differentiation of mesenchymal stem cells toward vascular endothelial cells stimulated by biphasic calcium phosphate ceramic," *Regenerative Biomater.*, vol. 5, no. 3, pp. 129–139, 2018.
[23] B. D. James and J. B. Allen, "Vascular endothelial cell behavior in complex mechanical microenvironments," *ACS Biomater. Sci. Eng.*, vol. 4, no. 11, pp. 3818–3842, 2018.
[24] M. Sorelli, A. Perrella, and L. Bocchi, "Detecting vascular age using the analysis of peripheral pulse," *IEEE Trans. Biomed. Eng.*, vol. 65, no. 12, pp. 2742–2750, Dec. 2018.
[25] Q. Fu, F. Shao, and M. Santello, "Inter-limb transfer of grasp force perception with closed-loop hand prosthesis," *IEEE Trans. Neural Syst. Rehabil. Eng.*, vol. 27, no. 5, pp. 927–936, May 2019.
[26] C. Veinidis, A. Danelakis, I. Pratikakis, and T. Theoharis, "Effective descriptors for human action retrieval from 3D mesh sequences," *Int. J. Image Graph.*, vol. 19, no. 3, pp. 1950018–1950030, 2019.
[27] A. S. Shadrina, M. A. Smetanina, K. S. Sevost'yanova, A. I. Shevela, E. I. Seliverstov, E. A. Zakharova, E. N. Voronina, E. A. Ilyukhin, I. A. Zolotukhin, A. I. Kirienko, and M. L. Filipenko, "Polymorphism of matrix metalloproteinases genes MMP1, MMP2, MMP3, and MMP7 and the risk of varicose veins of lower extremities," *Bull. Exp. Biol. Med.*, vol. 163, no. 5, pp. 650–654, 2017.
[28] A. J. J. Ijsselmuiden, C. Simsek, A. G. van Driel, D. Bouchez, G. Amoroso, P. Vermeersch, and P. P. Karjalainen, "Comparison between the STENTYS self-apposing bare metal and paclitaxel-eluting coronary stents for the treatment of saphenous vein grafts (ADEPT trial)," *Netherlands Heart J.*, vol. 26, no. 2, pp. 94–101, 2018.
[29] S. Zhang and S. Melander, "Varicose veins: Diagnosis, management, and treatment," *J. Nurse Practitioners*, vol. 10, no. 6, pp. 417–424, 2014.
[30] G. M. Roth, Z. E. Holcomb, B. Brown, J.-D. Fine, and G. Jennifer, "Resistance to narrowband ultraviolet B therapy over varicose veins in two cases of generalized vitiligo," *J. Dermatol. Nurses Assoc.*, vol. 9, no. 3, pp. 139–140, 2017.
[31] Z. Qu, T. Wang, S. An, and L. Liu, "Image seamless stitching and straightening based on the image block," *IET Image Process.*, vol. 12, no. 8, pp. 1361–1369, Aug. 2018.
[32] H.-F. Yang, K. Lin, and C.-S. Chen, "Supervised learning of semantics-preserving hash via deep convolutional neural networks," *IEEE Trans. Pattern Anal. Mach. Intell.*, vol. 40, no. 2, pp. 437–451, Feb. 2018.
[33] B. Pourbabaee, M. J. Roshtkhari, and K. Khorasani, "Deep convolutional neural networks and learning ECG features for screening paroxysmal atrial fibrillation patients," *IEEE Trans. Syst., Man, Cybern. Syst.*, vol. 48, no. 12, pp. 2095–2104, Dec. 2018.
[34] Y. Liang, Z. Tang, M. Yan, and J. Liu, "Object detection based on deep learning for urine sediment examination," *Biocybernetics Biomed. Eng.*, vol. 38, no. 3, pp. 661–670, 2018.
[35] R. Touati and M. Mignotte, "An energy-based model encoding nonlocal pairwise pixel interactions for multisensor change detection," *IEEE Trans. Geosci. Remote Sens.*, vol. 56, no. 2, pp. 1046–1058, Feb. 2018.
[36] X. Wu, R. He, Z. Sun, and T. Tan, "A light CNN for deep face representation with noisy labels," *IEEE Trans. Inf. Forensics Security*, vol. 13, no. 11, pp. 2884–2896, Nov. 2018.
[37] J. Lin, L. Xiao, and T. Wu, "Face recognition for video surveillance with aligned facial landmarks learning," *Technol. Health Care*, vol. 26, no. S1, pp. 169–178, 2018.
[38] O. Kotb, M. Ghandhari, R. Eriksson, and V. K. Sood, "On small signal stability of an AC/DC power system with a hybrid MTDC network," *Electr. Power Syst. Res.*, vol. 136, pp. 79–88, Jul. 2016.
[39] J. Zhu, H. Zeng, Y. Du, Z. Lei, L. Zheng, and C. Cai, "Joint feature and similarity deep learning for vehicle re-identification," *IEEE Access*, vol. 6, pp. 43724–43731, 2018.
[40] R. U. Khan, X. Zhang, and R. Kumar, "Analysis of ResNet and GoogleNet models for malware detection," *J. Comput. Virol. Hacking Techn.*, vol. 15, no. 1, pp. 29–37, 2019.
[41] W. Shi, Y. Gong, X. Tao, D. Cheng, and N. Zheng, "Fine-grained image classification using modified DCNNs trained by cascaded softmax and generalized large-margin losses," *IEEE Trans. Neural Netw. Learn. Syst.*, vol. 30, no. 3, pp. 683–694, Mar. 2019.

RUIZONG ZHU graduated from the Zhangjiakou of Medical Laboratory, Medical College, in 1999. He is currently with the Department of Clinical Laboratory, Dingzhou People's Hospital. His research interests include biochemistry and immunology.

HUIPING NIU graduated from Central South University, in 2005. She is currently with the Endoscopy Center, The Second Hospital of Hebei Medical University. Her research interests include disinfection and nursing of endoscopy.

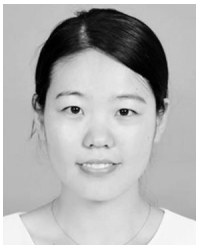

NINGNING YIN graduated from the Hebei United University of Medical Imageing, in 2017. She is currently with the Department of Ultrasound, The Second Hospital of Hebei Medical University. Her research interests include heart, abdomen, small organ, and especially vascular of ultrasonogrphy.

TIANJIAO WU graduated from the Hebei North University of Medical lmaging, in 2018. She is currently with the Department of Ultrasound, The Second Hospital of Hebei Medical University. Her research interests include heart, abdomen, small organ, and especially elastosonography of ultrasonogrphy.

YAPEI ZHAO graduated from the Medical College, Nantong University of Clinical Medical, in 1998. She is currently with the Department of Ultrasound, The Second Hospital of Hebei Medical University. Her research interests include abdomen, small organ, and especially vascular of ultrasonogrphy.